LAWRENCE
LIVERMORE
NATIONAL
LABORATORY

LLNL-JRNL-773415

PUSHERED SINGLE SHELL IMPLOSIONS FOR MIX AND RADIATION TRAPPING STUDIES USING HIGH-Z LAYERS ON NATIONAL IGNITION FACILITY*

E. L. Dewald, J. Pino, R. E. Tipton, J. D. Salmonson, J. Ralph, E. Hartouni, S. F. Khan, R. Hatarik, D. Thorn, V. A. Smalyuk, R. Sasks, M. Wang, A. Nikroo, N. Rice, S. MACLAREN, C. Young, S. Prisbey, B. Remington, F. Graziani

May 2, 2019

Physics of Plasmas

Disclaimer

PUSHERED SINGLE SHELL IMPLOSIONS FOR MIX AND RADIATION TRAPPING STUDIES USING HIGH-Z LAYERS ON NATIONAL IGNITION FACILITY

E.L. Dewald[1], J.E. Pino[1], R.E. Tipton[1], J.D. Salmonson[1], J. Ralph[1], E. Hartouni[1], S.F. Khan[1], R. Hatarik[1], C.V. Young[1], D. Thorn[1], V.A. Smalyuk[1], R. Sacks[2], A. Nikroo[1], N. Rice[3], S.A. MacLaren[1], S. Prisbey[1], B.A. Remington,[1] F. Graziani[1]

[1]*Lawrence Livermore National Laboratory, P.O. Box 808, Livermore, California 94550 USA*
[2]*Los Alamos National Laboratory, Los Alamos, New Mexico 87545, USA*
[3]*General Atomics, San Diego, California 92186, USA*

Abstract
Pushered Single Shells (PSS) are an alternative approach to Inertial Confinement Fusion (ICF) implosions that employ high-Z material in the innermost capsule layer (pusher) as a means to enhance radiation trapping and lower core ignition requirements. However, adding high-Z material can also increase losses due to mix, provide extra tamping, and make the capsule emission opaque to x-ray diagnostics. The first PSS implosions performed on the National Ignition Facility use plastic ablators with germanium (Ge) dopant as a high-Z surrogate in the pusher to isolate the effects of high-Z mix and radiation trapping without changing tamping. Using a 2-shock laser pulse, the PSS implosions are designed and symmetrized to reach 3.7 keV core temperatures. A low concentration (2.8%) Ge dopant is added to the innermost layer and the resulting effects on mix and x-ray opacity are observed. The method of separated reactants is used to infer information about mixing between the deuterated plastic pusher and the capsule fill gas (25% tritium) from the resulting nuclear DT reactions. Radiation transport is studied via capsule emission x-ray spectroscopy and imaging. Both nuclear and x-ray data corroborate the hypothesis that the addition of Ge strongly affects the mix region through radiation losses, but has a minimal effect on the core and the warm, un-mixed regions. Simulations using diffusive and turbulent mix models agree qualitatively with data, but quantitatve agreement may require hybrid mix models that can model the transitional regime between turbulence and diffusion. Simulations matching observables show increased core radiation trapping when Ge is added.

I INTRODUCTION

On the National Ignition Facility (NIF)[1], 192 laser beams with up to 2 MJ total energy are used to heat the interior of high-Z hohlraums[2,3]. The resulting x-ray drive ablatively implodes deuterium-tritium fuel filled capsules to a final hot spot radius of 25-60 μm, in order to achieve conditions needed for fusion ignition and burn. Figure 1 shows various capsule designs.

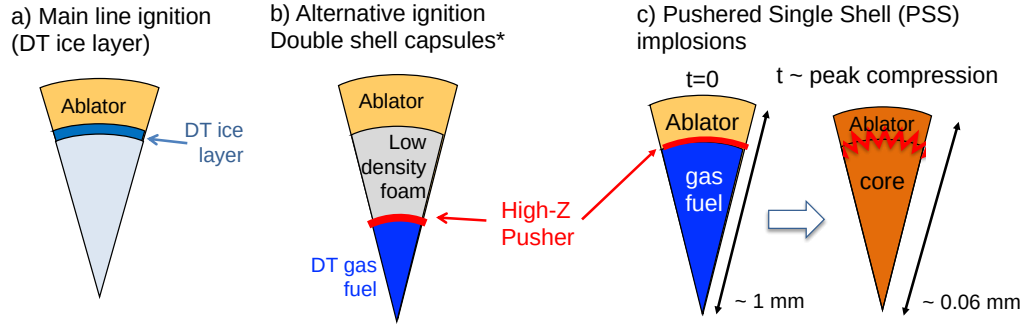

Figure 1. Implosion capsule designs for a) mainline ignition, b) double shells and c) pushered single shells.

For mainline inertial confinement fusion implosions on the NIF, the fuel consists of a solid DT ice layer (Fig. 1a) inside of a low-Z ablator shell[4]. The shell contains a mid-Z doped layer to shield the fuel against hohlraum radiation and electron preheat, allowing the compressed fuel to remain on a low adiabat and achive high compression. At peak compression ("stagnation"), the compressed core can experience significant energy loss due to electron conduction or bremsstrahlung radiation. In order to mitigate these losses, an alternative design class ("double shells"[5]) use gas fill fuel and a high-Z pusher to confine hot spot radiation losses through bremsstrahlung, achieving so-called radiation trapping (Fig. 1b). Trapping has the advantage of lowering the threshold temperature for self-sustaining ignition, which in turn relaxes capsule drive requirements, but it comes with three additional costs. First, the relatively poor ablative properties of higher-Z materials necessitate the use of a low-Z ablator, separated from the the high-Z "pusher" by a low-density foam. This allows efficient momentum coupling during the implosion, but adds greatly to the complexity of target assembly and fielding. Second, if too much pusher material mixes with the fuel, bremsstrahlung radiation is enhanced above what can be trapped, compromising ignition. This can be mitigated by the addition of a low-Z "anti-mix" layer between the core and the pusher. Lastly, by necessity the high-Z layer is sufficiently thick to trap radiation; this means that the ability to diagnose the core performance via x-ray radiography is greatly reduced.

Since adding a high-Z layer against the gas filled core also improves the core compression due to the increase in shell density (tamping), it is difficult to separate the effects of trapping from the improved compression. It is therefore essential to understand the interplay between mix and trapping at the fuel-pusher interface during peak compression. The effect of trapping is demonstrated computationally by a decrease in the difference between the core (matter) temperature and the radiation temperature during stagnation, which directly affects the core bremsstrahlung losses[4]. Due to the complexity of double shell targets, an intermediate platform, the Pushered Single Shell (PSS) implosion design[6,7] (Figure 1c) is used to order to validate these computational models. PSS implosions combine the ablator and a high-Z pusher in a single shell, offering an ease of manufacture and quality similar to mainline ICF capsules.

This work summarizes the first PSS studies on the NIF. In these experiments, germanium (Ge) is doped into the plastic as a high-Z pusher surrogate. At the low concentration used in these experiments (~2.5% by atomic weight), the Ge provides a significant increase in capsule opacity relative to pure plastic, while still allowing the capsule emission to be diagnosed. In addition to capsule x-ray radiography and spectroscopy, we study the pusher-fuel mix via nuclear diagnostics through the method of separated reactants[8]. The capsules contain deuterated inner layers co-located with the high-Z pusher surrogate, while the capsule gas fill consists of a 75/25% hydrogen-tritium (H/T) mixture. The 14-MeV neutron signal from DT reactions characterize the degree to which the pusher and fuel mix, while 5-10 MeV neutrons generated from TT reactions characterize the core. Additionally, neutrons from DD reactions characterize the warm un-mixed region of the implosion. The neutron signals and capsule x-ray emission at peak compression are measured both in the presence and absence of Ge dopant in the pusher. The results are compared to hydrodynamic simulations that include mix models.

This paper is organized as follows: Section II discusses the design of our PSS implosions, followed by tuning experiments aimed at characterizing and symmetrizing the shape of our implosions in

Section III. In Section IV we summarize the nuclear mix experiments, followed by capsule spectroscopy data presented in Section V. Section VI describes an empirical method used to infer the amount of capsule mass participating in mixing and demonstrates how the addition of Ge does not affect this mass. Finally, Sections VII and VIII discuss the effects of Ge dopant on radiation transport and mix, respectively. We offer conclusions and a future outlook in Section IX.

II THE DESIGN OF FIRST PSS IMPLOSIONS ON THE NIF

In order to isolate the core physics, the first PSS experiments on the NIF had to be relatively free of hydrodynamic feedthrough and shape effects. In order to achieve this, we start from the Two-Shock capsule design[9], shown in Figure 2. This implosion has demonstrated sufficient ablator mass remaining to shield the core from ablation front instabilities.

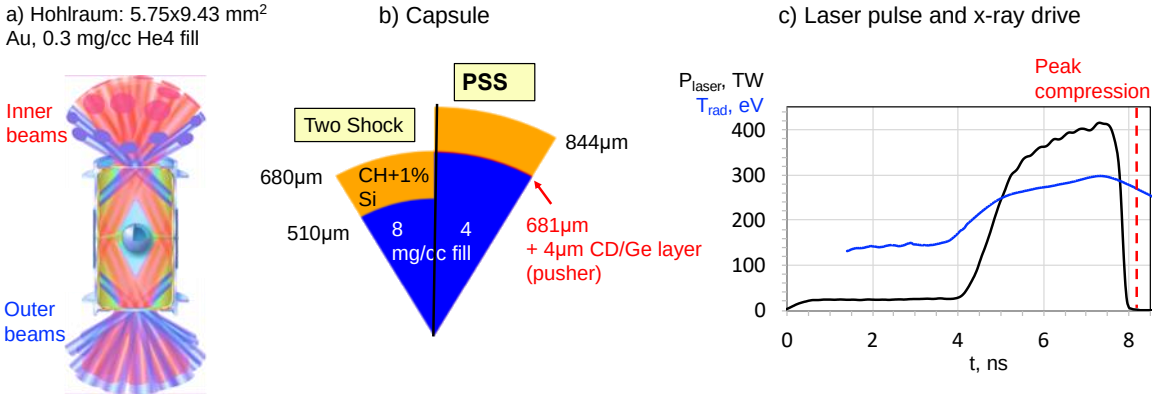

Figure 2 PSS implosion design: a) hohlraum and laser illumination, b) 2-Shock vs PSS capsule and c) laser pulse, hohlraum radiation temperature and capsule peak compression time.

We use a Au hohlraum with 5.75 mm diameter, 10.13 mm length and 3.37 mm diameter laser entrance holes, filled with 0.3 mg/cc He^4 gas fill for hohlraum wall tamping (Fig. 2a). The hohlraum is heated by all 192 beams from the NIF with a two-shock picketless pulse with 1.2 MJ total energy and 400 TW peak power. This generates a hohlraum peak radiation temperature of 300 eV, as measured by the Dante broadband soft x-ray spectrometer[10] (Fig. 2c). For mix and radiation trapping studies the capsule has a 4 μm thick Ge doped CH pusher as a high-Z surrogate at the shell-gas interface. Similar to two-shock implosions[8], the outer ablator surrounding the pusher consists of 165 μm of CH uniformly doped with 1% Si for shielding the core and pusher against hohlraum radiation preheat[11]. Two-shock implosions have shown that 10% of the initial ablator mass remains at stagnation, which is sufficient to mitigate ablation front instabilities feeding through to the gas-shell interface[9]. Furthermore, this implosion has a high adiabat[4,9], resulting in an implosion convergence of ~15 (defined as the ratio between initial capsule radius and the core radius at peak compression) and a stable ablation front with low instability growth.

The Ge dopant concentration in the pusher and capsule size are optimized based on 1D CALE[12] simulations of the capsule opacity at peak stagnation, shown in Figure 3. Simulations indicate that adding Ge dopant with a concentration > 2% results in significant increase in the capsule opacity at photon energies above 10 keV, as compared with no dopant. Overplotting idealized Planckian emission spectra for the core with the calculated opacity shows that the added Ge dopant could trap > 50% of the capsule radiation losses for core temperatures > 3 keV, but is not very effective at the ~2 keV core temperatures that are typical for Two-shock implosions[9]. Therefore, for PSS implosions we increase the capsule radius from 680 μm to 844 μm, while

maintaining the same gas fuel mass, ablator thickness and laser pulse (Fig. 2b). For a constant gas fuel mass, the core temperature is proportional to the mass-averaged shell kinetic energy at peak implosion velocity, which in turn scales linearly with the energy absorbed by the capsule from the hohlraum[4]. Since the hohlraum and laser drive profiles remain unchanged, the increase in capsule surface area results in a 60% increase in capsule absorbed energy and core temperature.

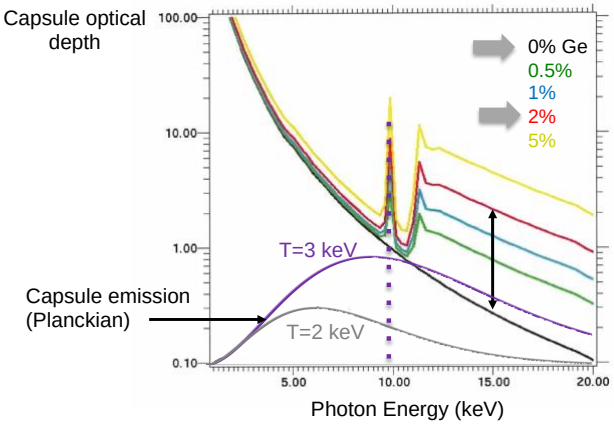

Figure 3 Simulated capsule optical depth at peak stagnation for various Ge dopant concentrations in the pusher (Fig. 2b) overlapped with approximate Planckian emission spectra from the core at 2 keV and 3 keV temperatures.

This allows the PSS core to reach temperatures of >3.2 keV (i.e. 160% of Two-Shock). The ablator mass remaining for PSS will be slightly lower than for 2-Shock capsules due to the higher implosion velocity required to increase the core temperature. To maintain the same gas fill fuel mass, we use a 4 mg/cc capsule fill density (2x less than Two-Shock) to compensate for the volume increasing by ~2x (Fig. 2b) with a 30% increase in inner capsule radius. These changes necessitated implosion tuning experiments to optimize implosion symmetry and verify that the shock trajectories are accurately captured in numerical simulations, as described in the next section.

III PSS IMPLOSION TUNING EXPERIMENTS

The first PSS implosions used Keyhole targets to validate and optimize the shock timing and minimize implosion asymmetry at early times (t = 0-4 ns, Fig. 2c). These capsules are filled with liquid D_2 and shock velocities are measured using a VISAR diagnostic[13]. Keyhole experiments with and without the Ge dopant (~2.8 at. wt.%) present in the inner 4 μm layer were also fielded to confirm that the dopant had negligible effect on the shock timing and strength.

Next, the implosion velocity and inflight shape were measured using streaked and time-gated backlit 2D radiography in a so-called convergent ablator (ConA) setup[14,15]. In these experiments, the capsule is filled with D_2 gas at 4 mg/cc and 0.8 mm large square holes are cut out of the hohlraum wall, replaced by high density carbon windows. 8 NIF laser beams from the outer cones are diverted to a 10 μm thick Fe backlighter foil to generate 6.7 keV Fe He-α x-rays[16]. This source is 12 mm away from the capsule midplane, in the direction normal to the hohlraum axis. The hot spot x-ray emission (photon energies > 6 keV) at stagnation and the inflight radiographs are both imaged with the same time-gated multi-channel plate based 4-strip imager[17] that employs several pinholes to record multiple images. The x-ray time resolved emission during peak compression (i.e. stagnation) time is measured by the SPIDER diagnostic[18].

Inflight shell and hot spot shapes are symmetrized (i.e. "tuned") by changing the inner-to-total laser beam power ratio (so-called "cone fraction") during the main pulse (Fig. 2c, t=4.5-7.5 ns) and by repointing the outer beams[13,14]. Figure 4a shows hot spot emission during peak compression ("stagnation") and the corresponding Legendre mode analysis for an untuned and a tuned implosion. Starting from an initial core P_2/P_0 Legendre mode asymmetry of 33% (P2=15 μm), we were able to achieve P2 symmetry by lowering the cone fraction during the main pulse from 0.26 to 0.21. Measured time histories of the capsule x-ray emission above 6 keV at peak compression shows similar stagnation times and ~150 ps burn duration (full width at half maximum, FWHM) with and without Ge dopant, consistent with the similar shell mass between the two cases.

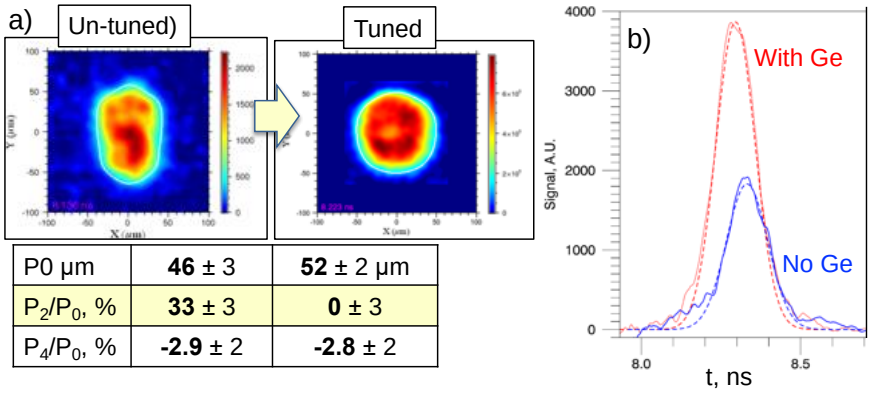

P0 μm	**46** ± 3	**52** ± 2 μm
P_2/P_0, %	**33** ± 3	**0** ± 3
P_4/P_0, %	**-2.9** ± 2	**-2.8** ± 2

Figure 4 a) > 6 keV hot spot emission recorded via pinhole imaging at peak compression and inferred asymmetry analysis for untuned and tuned implosions b) x-ray emission time history at peak compression for capsules with and without 2.8% Ge dopant in the inner layer.

The addition of Ge also results in a 2x brighter capsule x-ray emission at stagnation (Figure 4b). ConA radiography data is used to measure inflight shell shape and implosion trajectory as shown in Figure 5. The measured inflight shape of the radiograph limb minimum (P2 and P4 values) is conformal with the shape of the hot spot.

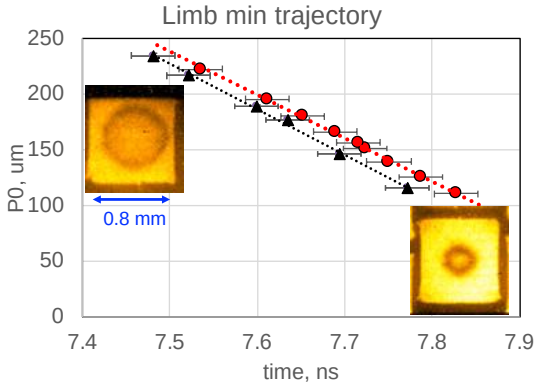

Figure 5 Sample inflight 2D ConA radiographs and corresponding inferred trajectory of limb minimum average radius (P0) for capsules with Ge dopant (red circles) and without Ge (black triangles).

The peak implosion velocity inferred from the limb minimum trajectory (Fig. 5) is the same within errors between the cases with Ge dopant (390 ±20 μm/ns) and without (410 ±20 μm/ns), consistent with the similar stagnation times (Fig. 4a). These values are among the highest for any capsule implosions on the NIF using a plastic ablator.

From 2DConA data, we infer that 8 ±1.5 % of the initial ablator mass remains when the shell reaches an inflight radius of 200 µm. This value is slightly below that observed in Two-Shock implosions (10%), as expected due to the increased implosion velocity[19]. 2D Ares[20] radiation-hydrodynamic simulations that recover this level of ablator mass remaining and a modest implosion convergence of 17 (= ratio of initial outer capsule radius, Fig. 2b, and hot spot P_0, Fig. 3) indicate that ablation front instability growth is very low (3x lower than ICF High Foot implosions[21]) and that the feedthrough of instabilities from the ablation front to the ablator-core interface is negligible (Figure 6).

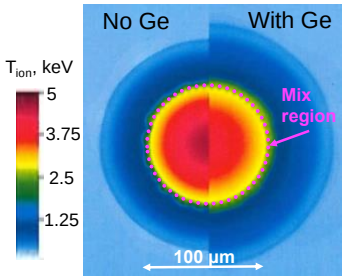

Figure 6 Ion temperatures at peak compression simulated using 2D Ares with and without Ge dopant. These simulations indicate that the PSS platform minimizes feedthrough from ablation front instabilities.

In summary, we achieved a PSS implosion that is symmetric (Fig. 4), has a short coasting time (Fig. 2) and has enough mass remaining to allow us to focus on our mix and trapping studies without interference from ablation front instabilities. Furthermore, several neutron time of flight (NToF) diagnostics[22] placed around the target record a high core ion temperature (T_{ion}) of 3.7 keV at stagnation. Adding the Ge dopant to the pusher lowers T_{ion} by a modest 0.2 keV. Despite the small effect on core temperature, the capsule emits 2x more radiation when Ge is added (Fig. 4b). With the implosion tuned to minimize any impact of shell asymmetry on mix, the PSS platform is well-suited to study mix and radiation trapping effects of the Ge high-Z surrogate.

IV PUSHER-GAS MIX INFERRED FROM NUCLEAR DATA

For studying gas-pusher mix we use the method of separated nuclear reactants[8]. The capsule is filled with 75%/25% (atomic fraction) hydrogen (H)/ tritium (T) gas at 4 mg/cc density (Fig. 2). The inner ~4 µm of the pusher contains deuterated plastic (CD) (Fig. 7a). Therefore the observed DT neutron yield resulting from deuterium in the shell and tritium in the core characterizes the gas-shell mix, the TT neutron yield characterizes the core conditions (Fig. 7b), and the DD neutron yield characterizes the warm, unmixed pusher region.

We quantify the amount of mix observed using the implosion mix figure of merit (FoM):

$$FoM = (Y_{DT}/Y_{TT})_{CD} - (Y_{DT}/Y_{TT})_{CH} \quad (1)$$

defined as the ratio of the mix yield (Y_{DT}) to the core yield (Y_{TT}) for the CD pusher, corrected for background DT signal arising from naturally occurring D content in the HT fill. Although the deuterium levels in the gas are very low (< 0.02 at%), past experiments[23] have shown that the DT background from the core can be significant, given that the core temperature is higher than that of the mix region. In order to characterize the DT background from the core, separate implosions are fielded without the CD layer (using CH pushers). An assumption is made that the details of the CH and CD implosions are identical, validated by the similar core TT yields that are measured on both. This allows us to compute an effective mix FoM as the difference between the figures of

merit [Eq. (1)] obtained from the experiments with CD and CH pushers. Additionally, the CH experiments provide a measurement of the core temperature from thermal broadening of the DT NToF signal. Since the TT reaction produces a two-neutron continuous energy spectrum, no thermal information can be directly extracted from the TT signal (Y_{TT} is defined as the number of measured neutrons in the 5-10 MeV particle energy range). The CH experiments demonstrate that the background DT signal is < 13% of the signal from the CD implosions and also establish the relative reproducibility of the TT core yield and DT background. An important detail to note is that the DD yield for CH pusher implosions is below detectable levels; hence, we conclude that the core contribution to the DD nuclear data for CD pushers is negligible.

The table in Figure 7c summarizes the recorded nuclear data which is an average value over 4 NToF detectors with various lines of sight around the capsule for our experiments with and without 2.8 at% Ge in the 4 μm thick pusher. As a general observation, the nuclear ion temperature (T_{ion}) decreases away from the core (3.7 keV without Ge), through the mix region (2.5 keV) and into the warm, unmixed region (1.5 keV). Data shows that the Ge dopant has a small effect on the core performance; as measured in the CH implosions, its presence reduces the core T_{ion} by only 6% and the TT yield by ~30%. The TT neutron yield reduction is fairly consistent with the TT reactivity dependence on temperature[24] ($\langle\sigma v\rangle \sim T_{ion}^4$), suggesting similar TT mass in the core for both experiments with and without Ge dopant in the pusher. The small effect of Ge on the core performance suggests that when adding Ge the core, losses are increased only by electron conduction from the core to the pusher-gas mix region.

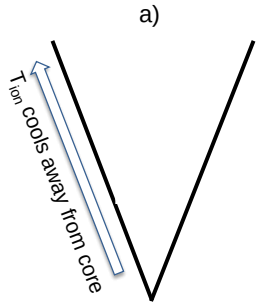

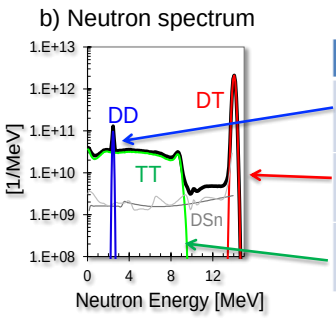

c) Neutron data

Reactants	Nuclear data	No Ge	2.8 % Ge	Error
D+D (warm, unmixed shell)	T_{ion}, keV	1.5	1.3	±0.15
	Y_{DD} x10^{11}	0.8	0.4	±0.03
D+T (MIX) (shell D + core T)	**T_{ion}, keV**	**2.5**	**1.9**	±0.15
	Y_{DT} x10^{11}	**34**	**8.3**	±0.3
T+T (core)	T_{ion}, keV	3.7	3.5	±0.1
	Y_{TT} x10^{11}	2.9	2.0	±0.4

Figure 7 Mix studies using the method of separate reactants: a) schematic of the capsule at peak compression, b) typical neutron spectrum and c) summary table of the nuclear data without and with Ge dopant in the pusher.

In contrast, the mix yield shows dramatic changes when Ge dopant is added: the DT T_{ion} decreases by 25% and the DT yield is reduced by 4x. Again, the yield decrease is consistent with the DT reactivity dependence on T_{ion} that scales as T_{ion}^5 at our ~2 keV mix temperatures[24], suggesting similar amounts of DT mix reactants with and without Ge dopant. A likely explanation for the significant decrease in mix region temperature is enhanced radiation cooling in the presence of the Ge dopant. This is corroborated by the observed 2x higher capsule x-ray emission with Ge (Fig. 4b), due to the significant change in capsule opacity at >7 keV photon energy (Fig. 3).
As in the case of the core, the Ge dopant has a small effect on the warm unmixed region as well, inferred from DD reactions. The DD reaction-weighted ion temperature T_{ion} decreases by 13%, and the DD neutron yield by 50%, consistent with the DD reactivity dependence on ion temperature that scales as $T_{ion}^{5.5}$ at the observed T_{ion} of 1.5 keV[24]. Similar to the core and mix regions, the consistent yield scaling with temperature suggests similar deuterium mass in the warm unmixed region, irrespective of the presence of Ge. The observation that Ge produces little effect

on the temperature of the warm unmixed region is consistent with the minor influence of Ge on the capsule opacity at $3kT_{ion}$= 4.5 keV photon energies (Fig. 3). It also supports the physical interpretation that the DD signal originates from a region a few optical depths away from the core, while the signal from DT mixing is derived from an area closer to the shell-gas interface where there is more sensitivity to opacity.

V CAPSULE X-RAY SPECTRA AT STAGNATION AND CORRELATION WITH NUCLEAR MIX DATA

In addition to the nuclear mix data (Fig. 7), we have recorded capsule x-ray emission spectra at stagnation, both with and without Ge dopant in the pusher. The capsule spectra are recorded by the NIF streaked spectrometer NXS[25] using an x-ray steak camera (DISC)[26] and time integrated, absolutely calibrated image plates. Figure 8 shows the recorded streaked x-ray spectra with and without Ge dopant in the pusher. In both cases with and without Ge dopant, the streaked spectra show a similar implosion burn duration with a FWHM of ~150 ps, in agreement with the > 6 keV emission measured by SPIDER[18] (Fig. 4). As expected for no Ge dopant in the pusher, only continuum emission is observed. A significantly brighter spectrum with noticeable Ge absorption and emission features is measured when adding Ge, consistent with the change in the capsule opacity (Fig. 3). The most prominent features in the spectrum (Fig. 8b) are the ionized Ge K-shell emission generated by the gas-pusher mix region and the 1s-2p absorption feature generated by core radiation being trapped in the warm, unmixed region (Fig. 7c).

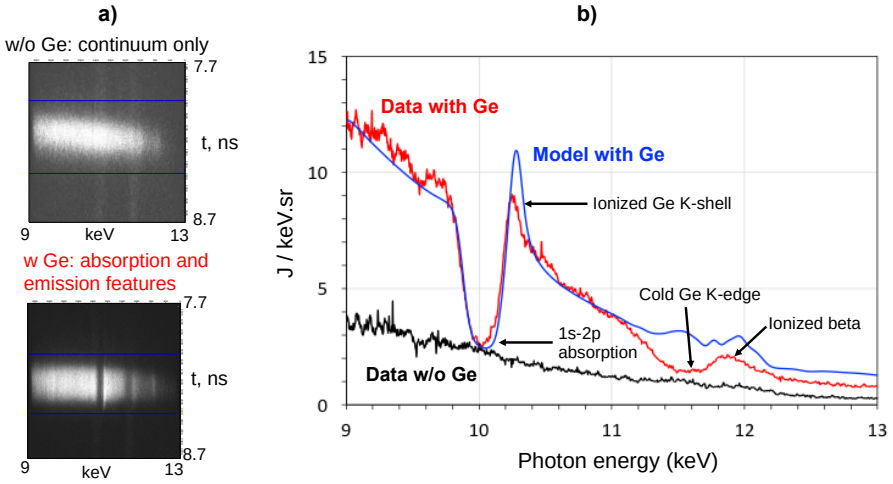

Figure 8 a) Streaked capsule spectra during implosion stagnation without Ge (top) and with Ge (bottom); b) time integrated spectra over the burn duration without Ge (black line), with Ge (red line) and post-processed from HYDRA capsule simulations with Ge using the CRETIN atomic physics code (blue line).

The emission spectrum at stagnation with Ge dopant is modeled with the atomic physics code CRETIN[27] using data extracted from 1D radiation-hydrodynamic HYDRA simulations[28] (blue line in Fig. 8b). We find that the modeled spectrum agrees fairly well with the measurement in terms of the absorption feature and ionized Ge K-shell emission. The simulations show that the absorption feature is caused by a warm (T_e=1.3 keV), dense (n_e=10^{25} cm^{-3}) region in the pusher. Given that ions and electrons are expected to be in thermodynamic equilibrium in this region, the modeled electron temperature is consistent with the measured nuclear DD T_{ion}=1.3 keV (Fig. 7). The measured and modeled spectra diverge in the region of ionized K-β emission at ~12 keV photon energies, likely due to simplifications in the Ge atomic physics model used in CRETIN.

Calculations with an improved atomic physics model are in progress. In a separate experiment[29], the core was characterized in the absence of Ge using emission spectroscopy of a Kr tracer (0.01 at%) added to the capsule fill. Using an isobaric core approximation, we inferred an electron temperature of 3.7 keV, which is also consistent with the 3.7 keV nuclear core TT Tion (Fig. 7). We conclude that the capsule x-ray spectra are consistent with the nuclear data and validate the simulated capsule implosion hydrodynamics.

In addition to the diagnostic data discussed above, "monochromatic" x-ray imaging of the core emission was performed using a KBO[29] system connected to an x-ray gated camera[15], centered at the Ge K-shell emission energy of 10.3 keV (Fig.7) with a bandwidth of 2 keV. Since the recorded images are qualitatively similar with and without Ge dopant in terms of core size and spatial structure, and they resemble the spectrally integrated > 6 keV images (Fig. 4), the images are not included in this paper. Moreover, hydrodynamic simulations of these PSS implosions conducted with and without mix models (see next section) do not show qualitative differences in the core emission; hence, KBO images cannot be used to further diagnose mix.

VI GE DOPANT EFFECT ON THE GAS-PUSHER MIX MASS

As described above, the changes in the measured TT, DT and DD nuclear yields due to the addition of Ge are at first glance consistent with the inferred changes in reactivity due to local power-law fits evaluated at the measured ion temperatures, suggesting similar mass for the reactants. These are, however, rough estimates that may have large uncertainties. Following the method derived in Ref 8, we can use the nuclear and x-ray data to estimate the fraction of T from the core that is clean, (generating the core TT yield), and mixed (generating the DT yield). The density of T participating in mix is estimated assuming the core is isobaric with the mix region at the corresponding measured core and mix region ion temperatures. It follows that, for a 1.35:1 D:C ratio, the deuterated CD mass m_{CD} (in ng) that participates in mix is given by[8]:

$$m_{CD} = 1.2 \times 10^{-7} \frac{T_{mix}}{T_{core}} \frac{Y_{DT}}{\sqrt{Y_{TT}}} \frac{\sqrt{\langle \sigma v \rangle_{TT-core}}}{\langle \sigma v \rangle_{DT-mix}} \frac{\sqrt{\tau_{core}}}{\tau_{mix}} R^{3/2} \quad (2)$$

where T_{mix} is the measured mix DT T_{ion}, T_{core} is the core (TT) T_{ion} (measured using CH implosions), Y_{DT} and Y_{TT} are the measured neutron yields in units of 10^{13} (see table in Fig. 7c); $\langle \sigma v \rangle_{TT}$ and $\langle \sigma v \rangle_{DT}$ are the corresponding nuclear reactivities in cm^3/s [23], τ_{core} and $\tau_{(mix)}$ are the burn durations for the core and mix regions in ps, and R is the core radius in μm. We assume that the core and mix burn durations are the same, given by the SPIDER data (Fig. 4b), and that the core radius R can be extracted from the x-ray core image (Fig. 4a). It follows that the amount of CD pusher mass participating in mix is 0.37 ±0.1 μg with Ge, and 0.46 ±0.1 μg without Ge. These numbers are similar within uncertainties, indicating that the mass of mixed material is unchanged by the presence of Ge. This amount of mass is contained within the first 55 ±15 nm of the CD pusher, initially 4 μm thick. The analysis suggests that only ~0.15 μg of core T participates in mix, representing 3% of the initial capsule fill, implying that 97% of the mass of the core remains clean. These estimates provide strong indications that that the length scale for mixing is relatively short.

VII MIX DATA VS SIMULATIONS IN PSS IMPLOSIONS

In this section we describe preliminary efforts to simulate the nuclear performance of the PSS capsules. A full investigation into simulation calibration and model sensitivities will be discussed in a subsequent paper. Nuclear mix data is compared to two different radiation-hydrodynamic simulations that account for mix with different models:

- CALE simulations using a Reynolds-Averaged Navier Stokes (RANS) model[12]. This method assumes fully developed turbulence in the mixing region and performs an ensemble average. For this model, the length scale of the turbulent mixing that is required to match data is quite long, and mix significantly degrades the core yield.
- Ares simulations using a diffusive mix model based on solving the Multi-Component Navier Stokes (MCNS)[20] equations. Mix is calibrated with a multiplier on the diffusivity. This model tends to show mix acting over short length scales, with a mild effect on core performance.

All the simulations reported in this section are one-dimensional (1D) which is acceptable, given the symmetric shape of the PSS implosions (Fig. 3). Additional 2D Ares calculations (Fig. 6) that include models of realistic initial surface perturbations are in close agreement with 1D results.
In Figure 9, we compare the mix FoM (Eq. 1) obtained from experiments with and without Ge dopant to these simulations. As discussed in Section IV, the FoM contains a correction for the background DT yield measured from the CH pusher experiments. With this correction (~ 0.7 in the units of Fig. 9), a FoM of zero would represent the absence of mix. Experimentally, a significant (2.4x) decrease in the mix FoM was found when adding 2.8 at% Ge dopant to the pusher. While both simulation methods qualitatively reproduce the observed trend, neither are in close agreement with the data. The calculations with diffusive mix that match the DT/TT yield ratio for the case without Ge overpredict the mix FoM when Ge is added. CALE simulations matching the core yields and the ratio between FoMs for the cases with and without Ge overpredict the amout of DT mix, and estimate larger mix masses than suggested by the analysis in section VI. Additionally, both sets of simulations show a discrepancy in the DD nuclear data characterizing the warm, unmixed region, calculating a 50% higher DD yield and ~30% lower DD ion temperature than what was measured (Fig. 7).

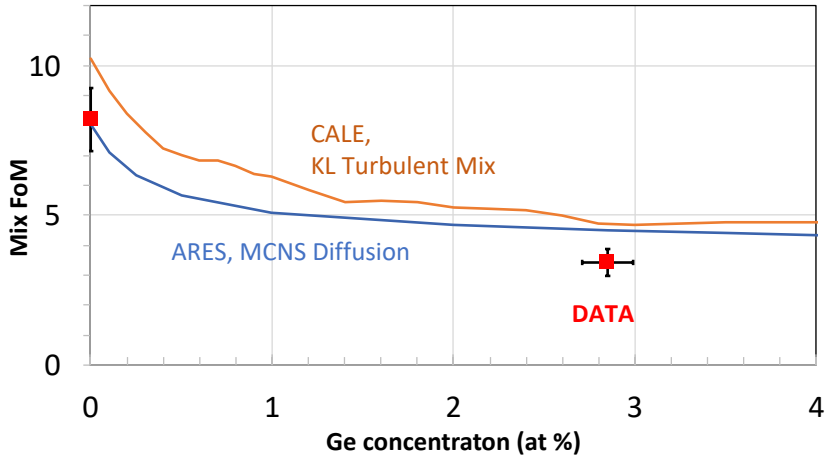

Figure 9 Mix figure of merit (FoM=$(Y_{DT}/Y_{TT})_{CD}$ - $(Y_{DT}/Y_{TT})_{CH}$) measured with and without Ge dopant in the pusher (data points in red). Simulations using CALE with RANS turbulent mix (brown line) and Ares with an MCNS diffusive mix model (blue line) achieve qualitative agreement with the data.

These simulations confirm our qualitative picture derived from the nuclear data (Fig. 7): while the Ge dopant has a relatively small effect on the core temperature, it reduces the temperature significantly in the mix region due to radiative losses, as suggested by the overall emission (Fig. 4) and x-ray spectra (Fig. 7).

One possible explanation for why neither model can match both Ge and no Ge cases is that the addition of Ge may change the balance between turbulent and diffusive mix in our PSS implosions. We can assess the relative importance of the two limits by calculating the reciprocal Knudsen number, i.e. the ratio between the capsule radius and the tritium ion mean free path λ_T at peak compression. When the reciprocal Knudsen number is large (>~10^4), turbulence is required to provide transport scales on the order of the capsule radius. In the small Knudsen limit (<~500), ions can diffuse easily across the capsule. Figure 10 shows the reciprocal Knudsen number as a function of radius as simulated by CALE. The plot indicates that the hot lower density core is diffusive as expected, while the warm unmixed region is turbulent. The mix region, however, with a width of ~25 μm, falls within the transitional range between diffusive and turbulent mix. When Ge dopant is added, the Knudsen number increases by ~3x.

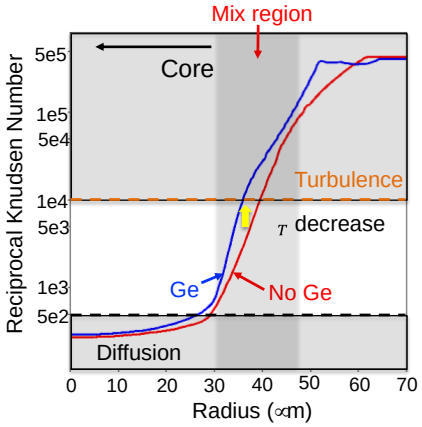

Figure 10 Reciprocal Knudsen number with Ge (blue line) and without Ge dopant (red line), as simulated by CALE with a turbulent mix model.

The significant change in reciprocal Knudsen number for such a low Ge concentration can be explained by its effect on the tritium ion mean free path, λ_T, in the mix region that scales as:

$$\frac{1}{\lambda_T} \cong \frac{1}{T_{mix}^2} \cdot \sum_i f_i \cdot Z_i^2 \qquad (3)$$

where T_{mix} is the average temperature in the mix region (i.e. DT T_{ion} in Fig. 7) and f_i is the atomic fraction of ion species i with an average ionization state Z_i. For no Ge dopant, the core T ions interact with the fully ionized (6+) pusher C atoms in the mix region and the sum in Eq. (3) evaluates to 18 for a 50% C atomic fraction. Here we neglect the pusher D ions, as their contribution to the mean free path is small due to the low (1+) ionization state. When adding 2.8 at% Ge to the pusher, the sum in Eq. (3) increases to 39 due to the high ionization state of the Ge (calculated to be ~26+). Accounting for the 25% measured decrease in mix temperature T_{mix} (Fig. 7), the ion mean free path λ_T decreases by >3x when adding Ge to the mix region. Thus, while a majority of the DT mix yield occurs near the core where the mixing is in the diffusive limit, the presence of Ge can drive the mixing toward turbulence. We conclude that a more sophisticated mix model that can resolve the transition between the two regimes may be needed to fully capture the effects of adding the Ge dopant. This will be investigated in future work.

VIII EFFECT OF ADDING GE DOPANT – RADIATION TRAPPING

We now employ our experimental data and simulation results to understand the effect of Ge dopant on mix and radiation transport from the core. Using a small amount of Ge dopant as a surrogate for a high-Z pusher presents several advantages as a starting point for validating models:

- The low amount of Ge has a small effect on the inflight capsule hydrodynamics, while providing a significant change in x-ray opacity and electron conduction (Fig. 3); previous PSS design studies[6,7] used high-Z pushers that simultaneously altered both radiation trapping and tamping, making it difficult to separate these two effects.
- While Ge affects the capsule opacity significantly above ~10 keV photon energies (Fig. 3), the concentration is low enough such that Ge emission and absorption can still be measured (Figs 3 and 7).
- Ge is partially ionized (26+), according to simulations validated by measured capsule x-ray spectra (Fig. 8), hence is a good surrogate for partially ionized higher-Z pushers, unlike fully ionized CH. At the same time, the observed x-ray spectra are dominated by simple K-shell emission and absorption that is easier to model, unlike the more complicated atomic structure of higher-Z materials.

The capsule emission at stagnation is significantly brighter when adding Ge dopant (Figs. 3 and 7), and the spectrum elucidates the balance between hot Ge participating in mix (through the ionized K-shell emission) and the warm unmixed Ge (through the absorption feature). It also provides a validation of the capsule hydrodynamics through the agreement with the modeled spectrum (Fig. 8). Specifically, the agreement in the depth and location of the 1s-2p absorption feature in photon energy space validates the density and ionization state of the simulated warm unmixed region. The simulated temperature of this region also matches the value experimentally inferred from thermal broadening of the DD neutron signal (Fig. 7). The ionized Ge emission originating from the mix region also agrees reasonably well with the simulations and shows a dominant He-α Ge line. This suggests that mixing Ge is localized at the gas-pusher interface with a ~2 keV core temperature, since no Ly-α emission (that would indicate higher temperatures) is observed. Finally, core spectroscopy using Kr tracers (not shown here) suggests an isobaric core temperature of 3.7 keV (in the absence of Ge), consistent with the measured nuclear T_{ion} (Fig. 7) and simulated average core temperature. Overall, we therefore observe consistency between x-ray spectroscopy, nuclear data and simulated capsule hydrodynamics.

The nuclear data (Fig. 7), complemented by the x-ray measurements, demonstrates the effect of the Ge dopant on radiation transport in various implosion regions:

- In the warm unmixed region (inferred from DD neutrons) there is a small decrease in temperature (13%) when Ge is added; this change is consistent with the modest effect of Ge on capsule opacity at the low x-ray emission centroid (3kT ~4 keV, Fig. 3).
- In the hotter mixed region (inferred from DT neutrons) the addition of Ge dopant has a significant cooling effect (25% decrease in temperature) due to enhanced radiative losses. The opacity enhancement with Ge is not significant at the mix region temperature (3kT ~6 keV emission centroid). Most of the enhanced capsule emission observed in the case with Ge dopant (Figs. 3, 7) is generated here, as suggested by the He-α emission (Fig. 8) requiring ~2 keV electron temperatures, consistent with the measured nuclear mix T_{ion}.
- Ge dopant has the smallest effect on the core region temperature (6% decrease); this could be explained by localized mixing that does not bring Ge deep into the core (an assumption which is corroborated by the absence of Ge Ly-α emission in Fig. 8). The probable

mechanism of enhanced energy loss is through electron conduction at the mix region when adding Ge, offset by enhanced radiation trapping. The additional opacity provided by the Ge dopant is very efficient at ~3.5 keV core temperatures (3kT ~11 keV core emission centroid, Fig. 3); as a result, the core averaged nuclear T_{ion} does not change much when adding Ge to the pusher.

In the core, the radiation flux will exchange energy with the electrons as given by[24]:

$$\frac{\partial E_e}{\partial t} = ac\rho\kappa_p(T_r^4 - T_e^4), \qquad (4)$$

where E_e is the thermal electron energy, a is a constant, c is the speed of light, ρ is the density, T_e is the electron temperature, and T_r is the equivalent radiation temperature of the photon flux. The Planck opacity κ_p or a fully ionized plasma is[24]:

$$\rho\kappa_p \approx 0.44\left(\frac{Z^*\rho}{A}\right)^2 \frac{1}{T_e^{3.5}}, \qquad (5)$$

where Z is the atomic number, A is the atomic mass, and the electron temperature is expressed in keV units. For many ICF implosions, the T_r term can be ignored because all emitted radiation leaves the core, never to return. However, if the fuel is surrounded by an opaque pusher, the pusher heats from both radiation and electron heat conduction coming from the hot spot (more by conduction than radiation). Once heated, the pusher can radiate some this heat back into the hot spot. In this case the T_r term is no longer negligible. The electron energy loss is decreased when the radiation flux ~T_r^4 increases (Eq. [4]), reaching so-called radiation trapping and permitting ignition at lower core temperatures.

While not directly measured, enhanced radiation trapping can be inferred from the data and corroborated by simulations that match the observables. The measured outward capsule x-ray emission (Fig. 4b) is enhanced by 2x when Ge is added and is generated by the hot mix region (Fig. 8). Therefore it is reasonable to assume that the radiation inward from the mix region into the core (T_r^4 factor in Eq.[4]) is also increasing by at least the same amount with Ge. The increased photon radiation flux in the core returns some of the lost energy to the core electrons per Eq. (4), enhancing radiation trapping. Figure 11 shows 1D CALE calculations of the escaping > 6 keV radiation, as well as radial lineouts of matter and radiation temperatures during peak compression with and without Ge dopant.

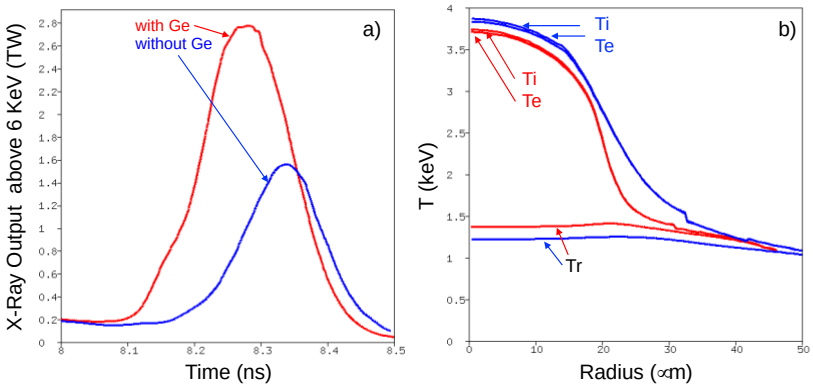

Figure 11 1D CALE calculations of PSS implosions. (a) Total capsule x-ray emission > 6keV with Ge (red) and without Ge dopant (blue), showing a ~2x increase in x-ray output from the addition of Ge. (b) Radial lineouts of electron temperature, Te, ion temperature, Ti and radiation temperature, Tr, at peak compression for cases with Ge (red) and without Ge (blue).

Figure 11 show that the escaping radiation doubles when adding Ge for burn durations of ~150 ps, consistent with the data (Fig. 4b). When Ge is added, the peak matter temperature in the core

decreases by ~5% (consistent with the measured nuclear T_{ion} Fig. 7) and the core radiation temperature increases by ~20%, suggesting enhanced radiation trapping. We also note that the gradient of the matter temperature increases with the addition of Ge (Fig. 11b) , another hallmark of enhanced radiation trapping. In this specific CH/Ge capsule design, the core electron energy exchange (Eq. [4]) does not change significantly, since the electron temperature is considerably higher than the radiation temperature (Fig. 11). Nevertheless, the photon flux factor T_r^4 nearly doubles when Ge is added.

In conclusion, data shows that Ge dopant in the pusher remains localized in the mix region, where it significantly increases radiation losses. Additional core losses through electron conduction at the core-mix region boundary are offset by Ge enhanced radiation trapping effects, leaving the core largely unchanged when adding Ge. Ares and CALE simulations show similar qualitative effects of dopant vs no dopant behavior on mix (Fig. 10) and radiation trapping (Fig. 11), with the notable difference that the mix width in Ares is shorter by >10x.

IX Outlook

In this work, we describe the design, tuning, and execution of the first pushered single shell (PSS) implosions on the NIF. In this first iteration, we added a low concentration of Ge to the pusher as a surrogate for higher-Z materials and investigate the resulting effects on pusher-gas mix and radiation trapping. These PSS implosions are derived from the hydrodynamically stable Two-Shock design, with an increased capsule radius to enhance energy coupling to the capsule. The core temperature is >3 keV, an energy regime in which the 2.8 at% Ge dopant in the pusher increases capsule opacity significantly. Mix studies using deuterated plastic shells show that adding a low amount of Ge to the inner pusher layer strongly affects the mix region, where radiation losses increase, while leaving the core and the warm unmixed regions largely unchanged. Capsule x-ray spectra validate simulations of implosion hydrodynamics and agree with nuclear measurements. Simulations incorporating models of turbulent and diffusive mix qualitatively reproduce the trends observed in the data between the cases with and without Ge dopant; however, the measured change in mix behavior is larger than simulated. This could be explained by the mix region existing in a transition regime between turbulence and diffusion, and will be the subject of future computational investigations. Despite adding only a low concentration of Ge, we estimate that this produces a more turbulent mix region and resulting decrease of the ion mean free path, leaving mix mass unchanged. Data and simulations matching the observables show evidence of increased core radiation trapping when Ge is added.

Further PSS implosion experiments moving towards higher-Z pushers are currently underway on the NIF. These designs use Be outer ablators with a smooth concentration gradient that reach up to 50% Cr dopant in the inner layer. 1-2 μm of pure Be is placed at the pusher-gas interface as an anti-mix layer to mitigate core losses due to mix. Simulations with mix models calibrated to the present data (Fig. 9) are used to optimize capsule design and demonstrate enhanced radiation trapping. For higher-Z pushers, less core radiation escapes, so these experiments rely heavily on nuclear data to assess implosion performance.

ACKNOWLEDGEMENT

This work performed under the auspices of the U.S. DOE by Lawrence Livermore National Laboratory under Contract DE-AC52-07NA27344.

References

[1]G.H. Miller, E.I. Moses, C.R. Wuest, *Nucl. Fusion* **44,** 228 (2004).

[2]G.D. Tsakiris, J. Massen, R. Sigel, F. Lavarenne, R. Fedosejevs, J. Meyer-ter-Vehn, K. Eidmann, S. Witkowski, H. Nishimura, Y. Kato, H. Takabe, T. Endo, K. Kondo, H. Shiraga, S. Sakabe, T. Jitsuno, M. Takagi, C. Yamanaka, S. Nakai, *Phys. Rev. A* **42**, 6188 (1990); W.A. Stygar, R.E. Olson, R.B. Spielman, R.J. Leeper, *Phys. Rev. E* **64**, 026410 (2001).

[3]F. Phillippe, A. Casner, T. Caillaud, O. Landoas, M.C. Monteil, S. Liberatore, H.S. Park, P. Amendt, H. Robey, C. Sorce, C.K. Li, F. Seguin, M. Rosenberg, R. Petrasso, V. Glebov, C. Stoeckl, *Phys. Rev. Lett.* **104**, 035004 (2010).

[4]J.D. Lindl, P. Amendt, R.L. Berger, S.G. Glendinning, S.H. Glenzer, S.W. Haan, R.L. Kauffman, O.L. Landen, *Phys. Plasmas* **11**, 339 (2004).

[5]P. Amendt C. Cerjan, A. Hamza, D.E. Hinkel, J.L. Milovich, H.F. Robey, *Phys. Plasmas* **14**, 056312 (2007).

[6]M.M. Basko, Nucl. Fusion **30** (12), 2443 (1990).

[7]J. Milovich, P. Amendt, M. Marinak, H.F. Robey, *Phys. Plasmas* **11**, 1552 (2004).

[8]D. Casey, V.A. Smalyuk, R.E. Tipton, J.E. Pino, G.P. Grim, B.A. Remington, D.P. Rowley, S.V. Weber, M. Barrios, L.R. Benedetti, *et al*, *Phys. Plasmas* **21**, 092705 (2014).

[9]S.F. Khan, S.A. Maclaren, J.D. Salmonson, T. Ma, G.A. Kyrala, J.E. Pino, J.R. Rygg, J.E. Field, R. Tommasini, J.E. Ralph, *et al*, *Phys Plasmas* **23**, 042708 (2016).

[10]E.L. Dewald, K.M. Campbell, R.E. Turner, J.P. Holder, O.L. Landen, S.H. Glenzer, R.L. Kauffman, L.J. Suter, M. Landon, M. Rhodes, D. Lee, *Rev. Sci. Instrum*. **75**, 3759 (2004).

[11]E.L. Dewald, R. Tommasini, N.B. Meezan, O.L. Landen, S. Khan, R. Rygg, J. Field, A.S. Moore, D. Sayre, A.J. MacKinnon, L.F. Berzak Hopkins, L. Divol, S. LePape, A. Pak, C.A. Thomas, M. Farrell, A. Nikroo, O. Hurricane, *Phys. Plasmas* **25**, 092702 (2018).

[12]G. Dimonte, R. Tipton, *Phys. Fluids* **18**, 085101 (2006).

[13]O.L. Landen, T.R. Boehly, D.K. Bradley, D.G. Braun, D.A. Callahan, P.M. Celliers, G.W. Collins, E.L. Dewald, L. Divol, S.H. Glenzer, A. Hamza, D.G. Hicks, N. Hoffman, N. Izumi, O.S. Jones, R.K. Kirkwood, G.A. Kyrala, P. Michel, J. Milovich, D.H. Munro, A. Nikroo, R.E. Olson, H.F. Robey, B.K. Spears, C.A. Thomas, S.V. Weber, D.C. Wilson, M.M. Marinak, L.J. Suter, B.A. Hammel, D.D. Meyerhofer, J. Atherton, J. Edwards, S.W. Haan, J.D. Lindl, B.J. MacGowan, E. I. Moses, *Phys. Plasmas* **17**, 056301 (2010).

[14]J.R. Rygg, O.S. Jones, J.E. Field, M.A. Barrios, L.R. Benedetti, G.W. Collins, D.C. Eder, M.J. Edwards, J.J. Kroll, O.L. Landen *et al*, *Phys. Rev. Lett.* **112**, 195001 (2014).

[15]E.L Dewald, R. Tommasini, A. Mackinnon, A. MacPhee, N. Meezan, R. Olson, D. Hicks, S. LePape, N. Izumi, K. Fournier, M.A. Barrios, S. Ross, A. Pak, T. Döppner, D. Kalantar, K. Opachich, R. Rygg, D. Bradley, P. Bell, A. Hamza, B. Dzenitis, O.L. Landen, B. MacGowan, K. LaFortune, C. Widmayer, B. Van Wonterghem, J. Kilkenny, M.J. Edwards, J. Atherton, E.I. Moses, *J. Phys: Conf. Series* **688**, 012014 (2016).

[16]J. Workman, G. Kyrala, *Proc. SPIE* **4504**, 168 (2001); M.A. Barrios, K.B. Fournier, S.P. Regan, O. Landen, M. May, Y.P. Opachich, K. Widmann, D.K. Bradley, G.W. Collins, *High. En. Dens. Phys.* **9**, 626 (2013).

[17]G.A. Rochau, J.E. Bailey, G.A. Chandler, T.J. Nash, D.S. Nielsen, G.S. Dunham, O.F. Garcia, N.R. Joseph, J.W. Keister, M.J. Madlener, D.V. Morgan, K.J. Moy, M. Wu, *Rev. Sci. Instrum* **77**, 10E323 (2006); D.K Bradley, P.M. Bell, J.D. Kilkenny, R. Hanks, O. Landen, P.A. Jaanimagi, P.W. Mckenty, C.P. Verdon, *Rev. Sci. Instrum.* **63**, 4183 (1992).

[18]S.F. Khan, P.M. Bell, D.K. Bradley, S.R. Burns, J.R. Celeste, L.S. Dauffy, M.J. Eckart, M.A. Gerhard, C. Hagmann, D.I. Headley, J.P. Holder, N. Izumi, M.C. Jones, J.W. Kellogg, H.Y. Khater, J.R. Kimbrough, A.G. Macphee, Y.P. Opachich, N.E. Palmer, R.B. Petre, J.L. Porter, R.T. Shelton, T.L. Thomas, J.B. Worden, *Proc. SPIE* **8505**, 850505 (2012).
[19]D.G. Hicks, N.B. Meezan, E.L. Dewald, A.J. MacKinnon, R.E. Olson, D.A. Callahan, T. Doeppner, L.R. Benedetti, D.K. Bradley, P.M. Celliers, *et al, Phys. Plasmas* **19**, 122702 (2012).
[20]R.M. Darlington, T.L. McAbee, G. Rodrigue, *Comput. Phys. Commun*. **135**, 58 (2001).
[21]O.A. Hurricane, D.A. Callahan, D.T. Casey, P.M. Celliers, C. Cerjan, E.L. Dewald, T.R. Dittrich, T. Döppner, D.E. Hinkel, L.F. Berzak Hopkins, J.L. Kline, S. Le Pape, T. Ma, A.G. MacPhee, J.L. Milovich, A. Pak, H.-S. Park, P.K. Patel, B.A. Remington, J.D. Salmonson, P.T. Springer, R. Tommasini, *Nature* **506**, pp. 343-348 (2014).
[22]V.Y. Glebov, D.D. Meyerhofer, T.C. Sangster, C. Stoeckl, S. Roberts, C.A. Barrera, J.R. Celeste, C.J. Cerjan, L.S. Dauffy, D.C. Eder et al, *Rev. Sci. Instrum.* **77**, 10E715 (2006).
[23]G.A. Kyrala, J.E. Pino, S.F. Khan, S.A. Maclaren, T. Ma, L. Masse, R. Tipton, P.A. Bradley, J.R. Rygg, J.E. Field, *et al*, *Phys. Plasmas* **25**, 102702 (2018).
[24]S. Atzeni, J. Meyer-ter-Vehn, *The Physics of Inertial Confinement Fusion*, p. 20, Oxford University Press (2004).
[25]F. Perez, G.E. Kemp, S.P. Regan, M.A. Barrios, J. Pino, H. Scott, S. Ayers, H. Chen, J. Emig, J.D. Colvin, M. Bedzyk, M.J. Shoup III, A. Agliata, B. Yaakobi, F.J. Marshall, R.A. Hamilton, J. Jaquez, M. Farell, A. Nikroo, K.B. Fournier, *Rev. Sci. Instrum*. **85**, 11D613 (2014).
[26]Y.P. Opachich, D.H. Kalantar, A.G. Macphee, J.P. Holder, J.R. Kimbrough, P.M. Bell, D.K. Bradley, B. Hatch, G. Brienza-Larsen, C. Brown, *et al*, *Rev. Sci. Instrum*. **83**, 125105 (2012).
[27]H.A. Scott, *J. Quant. Spec. and Rad. Transfer*, **71,** pp. 689-701 (2001)
[28]M.M. Marinak, G. D. Kerbel, N. A. Gentile, T.R. Dittrich, S. W. Haan, *Phys. Plasmas* **8**, 2275 (2001).
[29] D.B. Thorn, M.J. Macdonald, A.G. MacPhee, K. LeChien, E. Dewald, D. Liedahl, V. Smalyuk, C. Yeamans, R. Hatarik, M.B. Schneider, et al, *"Mass-temperature distribution within ICF implosions on the National Ignition Facility", Workshop on Radiative Properties of Hot Dense Matter (RPHDM)*, Hamburg, Germany (2018).
[30]L.A. Pickworth, J. Ayers, P. Bell, N.F. Brejnholt, J.G. Buscho, D. Bradley, T. Decker, S. Hau-Riege, J. Kilkenny, T. McCarville,T. Pardini, J. Vogel, C. Walton, *Rev. Sci. Instrum*. **87**, 11E316 (2016).
[31] B.J. Olson, J. Greenough, *Phys. Fluids* **26**, 044103 (2014).

*This work performed under the auspices of the U.S. DOE by Lawrence Livermore National Laboratory under Contract DE-AC52-07NA27344.